Available online at www.sciencedirect.com
SCIENCE DIRECT®
Journal of Power Sources 119–121 (2003) 550–554
JOURNAL OF POWER SOURCES
www.elsevier.com/locate/jpowsour

Microprobe study of the effect of Li intercalation on the structure of graphite

Robert Kostecki*, Frank McLarnon
Lawrence Berkeley National Laboratory, Berkeley, CA 94720, USA

Abstract

The structural stability of graphite electrodes in Li-ion cells, which were cycled at room temperature and 60 °C was investigated. We observed gradual structural degradation of the graphite, which was most pronounced on the electrode surface but also extended into the bulk of the electrode. Graphite particles close to the Cu current collector remained almost unchanged, whereas those close to the electrode/electrolyte interface suffered significant structural damage. Structural degradation of the graphite led to an increased anode surface reactivity vs. the electrolyte. A thick layer of inorganic products from side reactions was observed on the disordered carbon areas of the anode.

Keywords: Li intercalation; Graphite anode; Carbon disordering; Solid electrolyte interphase (SEI)

1. Introduction

Most present-day commercial Li-ion batteries employ graphitic carbon-based negative electrodes (anodes). Electrochemical lithium intercalation into graphite and the accompanying formation of a solid electrolyte interphase (SEI) have been extensively studied and reported in the literature [1–4]. However, there remain unresolved issues regarding the mechanism of surface processes on graphite that are associated with irreversible charge consumption during the initial formation cycles and during subsequent cell cycling and/or storage. Although it is generally accepted that reduction of the electrolyte is primarily responsible for SEI layer formation, the mechanism and kinetics of this process are very complex and persist as a subject of controversy.

Raman spectroscopy is among the preferred methods for analysis of graphitic structures, because it provides structural information second only to X-ray diffraction. Although Raman spectroscopy is suited only for near-surface studies because of the high optical extinction coefficient of carbon, it is extremely sensitive to changes that disrupt the translational symmetry of graphite basal planes. Confocal Raman microscopy is a particularly powerful tool for the study of electrochemical interfaces because of its ability to examine either electrode surface features or the adjacent electrolyte at micrometer resolution. Some remarkable examples of the application of this technique to battery systems were presented by Rey and co-workers [5], who used it to monitor Li^+-ion concentration profiles in a polymer electrolyte; by Luo et al., who carried out in situ single-particle Raman microscopy studies of $LiMn_2O_4$ [6] and graphite [7] embedded in Au and Ni electrodes, respectively; and by Novák et al. [8,9], who conducted an in situ investigation of SEI layer formation on graphite.

We have used Raman microscopy and atomic force microscopy (AFM) to study the effect of structural changes which occur in graphitic materials during Li-ion cell cycling at ambient and elevated temperatures. We evaluated the near-surface and surface changes resulting from the exposure of graphitic electrodes to stresses associated with elevated temperature and numerous Li intercalation/deintercalation cycles, in terms of graphite structure disordering and SEI layer morphology, thickness, and composition change. We applied high-resolution Raman microscopy mapping, not only to survey the anode surface but also to image a cross-section of the anode, i.e. we recorded a Raman image of a section of the anode in the plane perpendicular to the anode current collector. These experiments allowed us to not only assess non-uniform structural damage induced in graphite but also detect the formation of non-homogeneous electrolyte decomposition products within the bulk of the anode. The results of this study established a correlation between graphite physico-chemical behavior and the corresponding experimental electrochemical data, and may be

* Corresponding author. Tel.: +1-510-486-6002; fax: +1-510-486-4995.
E-mail address: r_kostecki@ibl.gov (R. Kostecki).

0378-7753/03/$ – see front matter
doi:10.1016/S0378-7753(03)00287-8

helpful in theoretical modeling of Li-ion battery performance.

2. Experimental

Several 15 mAh Li-ion pouch cells were constructed from anodes and cathodes supplied by Quallion Corp. (Sylmar, CA) and Celgard 2500 separator sealed in an Al foil-laminated polymer film [10]. The cathode consisted of 84 wt.% $LiNi_{0.8}Co_{0.15}Al_{0.05}O_2$ (Fuji CA1505), 4 wt.% carbon black (Chevron), 4 wt.% SFG-6 (Timical), and 8 wt.% PVdF (Kureha) on Al foil. The anode was made of 92 wt.% MAG-10 graphite (Hitachi chemical) and 8 wt.% PVdF (Kureha) on Cu foil. Cells were vacuum-filled with 1 M $LiPF_6$ in EC/DEC electrolyte (LP40, EM Science). This cell chemistry is similar to that used in the Department of Energy Advanced Technology Development (ATD) Program generation-2 cells [11], except for the electrolyte.

Cell assembly, formation cycle, and cycling protocol (C/2 rate, 100% DOD between 3.0 and 4.1 V at ambient temperature and at 60 °C) are presented in detail [10]. The cell cycled at room temperature exhibited 33% capacity loss after 480 cycles, whereas the cell cycled at 60 °C lost 65% of its capacity after 140 cycles. After cycling, the pouch cells were fully discharged and disassembled in a He-atmosphere glovebox, and each component was washed in dimethyl carbonate for 24 h and dried at room temperature in vacuum. Small pieces of the anode were then transferred to sealed containers and analyzed by Raman microscopy and AFM.

An integrated Raman microscope system "Labram" made by ISA Groupe Horiba was used to analyze the structure and composition of the anodes. The excitation wavelength was supplied by an internal He–Ne (632 nm) 10 mW laser. The power of the laser beam was adjusted to 0.1 mW with neutral filters of various optical densities. The size of the laser beam at the sample was ~1.2 μm. Raman mapping of the anode surface and the anode cross-section was carried out across a typical 41 μm × 60 μm area at 0.7 μm lateral resolution, using a software-controlled motorized XY stage.

Atomic force microscopy images were recorded in contact mode using a Picoscan Molecular Imaging scanning probe microscope coupled with a ThermoMicroscopes, Inc. AFM electronic controller.

3. Results and discussion

Raman spectroscopy is a particularly useful tool for characterizing the near-surface structure of graphite because of its relatively large Raman scattering cross-section. A typical Raman spectrum of graphite consists of two E_{2g} active modes: a strong (G) band at ~1582 cm^{-1} and a weak band at 42 cm^{-1}, which is difficult to observe. However, decreasing intra-planar (L_a) and inter-planar (L_c) graphite

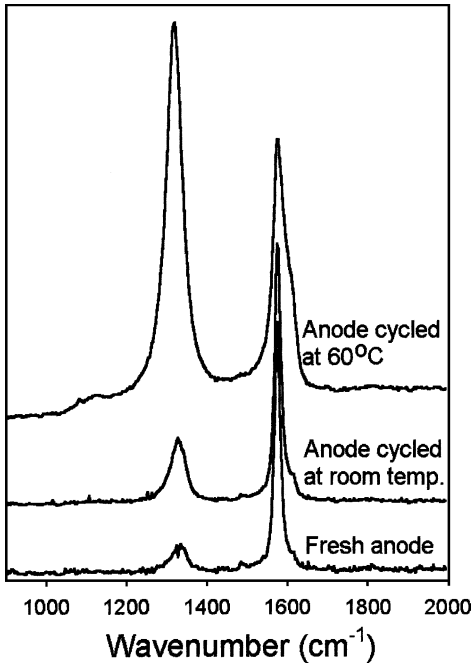

Fig. 1. Average Raman spectra of graphite anodes: lower curve, fresh anode; middle curve, anode cycled at room temperature; and upper curve, anode cycled at 60 °C.

microcrystallite dimensions always give rise to a new feature at ~1360 cm^{-1}. This (D) band, which is assigned to the A_{1g} mode, is associated with the breakage of symmetry occurring at the edges of graphite sheets. Thus, the more edges present, the more phonons that can result in Raman scattering, and the more intense the D band becomes. The relative intensity of the D band versus G band is attributed to increased carbon disorder, for example, in microcrystalline graphite [12]. Tuinstra and Koenig [13] showed that the ratio of D/G integrated peak intensities is inversely proportional to the intra-planar microcrystallite distance L_a.

Average Raman spectra from representative 42 μm× 60 μm areas of a fresh graphite anode, the anode cycled at room temperature, and the anode cycled at 60 °C are presented in Fig. 1. Two broad bands are present at ~1360 and ~1580 cm^{-1}. The relative D and G peak heights change noticeably for the anode cycled at room temperature, but most dramatic spectral change is observed for the anode cycled at 60 °C. The D band intensity increases substantially, the G band broadens significantly, and a new band at ~1620 cm^{-1}, which is typical of "severely disordered" carbonaceous materials [14], appears in the 60 °C spectrum. Interestingly, close examination of the Raman spectrum of the anode from the cell cycled at 60 °C reveals a series of small bands centered around ~1100 cm^{-1} (see Fig. 3), suggesting the presence of inorganic products arising from electrolyte decomposition.

The relative average intensity ratios of the D and the G bands increased for the cycled anodes, indicating that severe structural damage was induced into the graphite during cycling, especially at elevated temperature. To examine

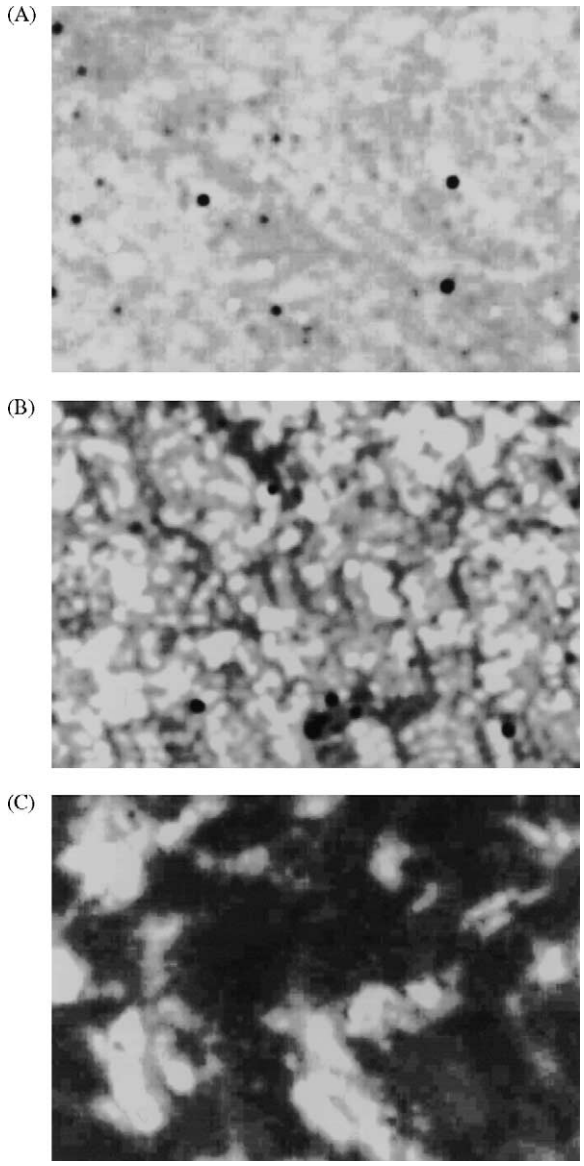

Fig. 2. Raman microscopy images of graphite anodes. (A): fresh anode, (B): cell cycled ~400 times at room temperature, (C): cell cycled ~140 times at 60 °C. White areas represent pure graphite, and dark gray areas indicate structural disorder. The small, black round spots visible on panel (A) are artifacts. Image size is 40 μm × 60 μm.

the extent of graphite structural damage, a series of Raman mapping experiments were carried out. Fig. 2 shows gray-scale-coded Raman images of the integrated intensity ratio of D/G carbon Raman bands collected from three 42 μm × 60 μm anode areas with 0.7 μm resolution. The D/G ratio is inversely proportional to the size of microparticles, and it increases with the extent of carbon disorder. The lighter the shade of gray on the image the more graphitic is the local anode structure, and conversely the darker the shade of gray the more disordered is the local anode structure. The Raman images of the graphite anodes reveal that graphite undergoes gradual structural degradation upon cycling. The fresh anode displays a fairly uniform graphitic structure with some local disorder, which appears mainly at the edges of graphite flakes. The increased prevalence of dark areas at the surface of the anode cycled at room temperature indicates and increased extent of local graphite structural degradation. In marked contrast, severe local structural disorder is observed in the anode from the cell cycled at 60 °C. Most of its surface became amorphous/disordered, with only a few local areas which retained the original graphitic structure. This Raman surface map of the anode shows clearly that not only does graphite structural degradation proceed in a non-uniform manner, but also that the process is greatly accelerated at elevated temperatures.

Note that the results shown in Fig. 2 apply only to the surface and near-surface regions of the anode surface, i.e. to the depth that the Raman excitation beam penetrates into the anode bulk. Shallow structural degradation of graphite is unlikely to influence significantly the overall reversible anode capacity. The effects of graphite surface modification and the alteration of particle morphology by mechanical milling [15], fluorination [16], and thermal treatment [17] on their electrochemical properties have been studied extensively. Such disordered carbons show very high reversible capacity (~700 Ah kg^{-1}); however, they typically exhibit dramatically increased (to more than ~350 Ah kg^{-1}) irreversible capacity loss, which is associated with the side reactions with the electrolyte during formation cycles.

Fig. 3 shows a series of Raman microscope spectra recorded at different locations on the surface of the anode cycled at 60 °C. Clear spectral evidence of new inorganic compounds was observed at locations where significant

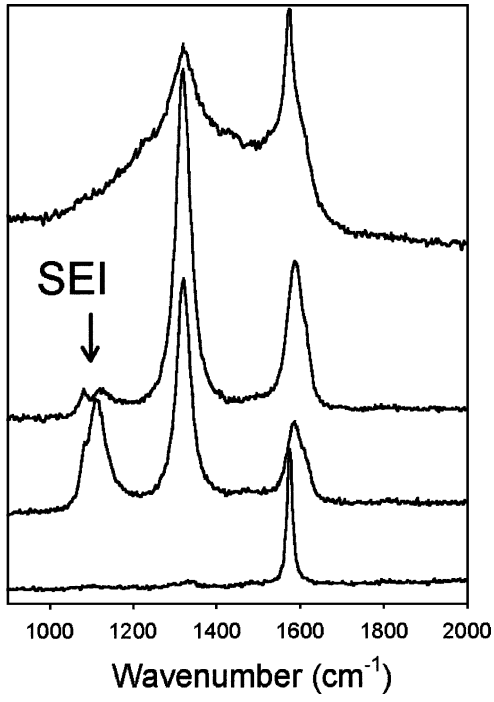

Fig. 3. Raman microscope spectra recorded form different locations on the surface of an anode from a cell cycled at 60 °C. The lowest curve is typical of undisturbed graphite.

graphite surface disorder was induced. The band at 1084 cm^{-1} is due to symmetric stretching vibrations of Li_2CO_3 [18], and a series of bands between 1100 and 1150 cm^{-1} can be assigned to vibrations of terminal groups such as $(PO_2)^-$ and $(PO_3)^-$ in polyphosphates [19]. Interestingly, no evidence of inorganic compounds was found on locations that retained a structure typical of undisturbed graphite. Gradual graphite disordering induced by lithium intercalation/deintercalation leads to an increased anode surface reactivity versus the electrolyte. A thick layer of inorganic products arising from side reactions accumulated on the disordered sites of the graphite anode, suggesting that structural changes in the electrode surface structure strongly affected the formation and composition of the SEI.

These results are confirmed by the ex situ AFM surface images which revealed significant changes in electrode topography (Fig. 4). The AFM image of the fresh electrode (A) shows randomly oriented graphite flakes with well-pronounced basal planes, steps, and edges; whereas the surface of the anode cycled at elevated temperature (B) displays nanocrystalline deposits which accumulated preferentially on graphite flake cross-sections, plane steps, and edges. Interestingly, there is no evidence of such nanocrystalline deposits on the graphitic planes.

To obtain more detailed information of the extent of structural damage in the anode as well as the electrolyte decomposition product distribution, we analyzed the structure and chemical composition of the anode cross-section. We cleaved the anode, and then imaged its cross-section via Raman microscopy. Fig. 5A shows a Raman graphite D/G ratio map of the anode cross-section. Cursory visual examination of the Raman map reveals severe structural damage in the anode bulk, signaled by the appearance of dark gray regions. In order to correlate the local graphite structure within the anode with distance from the electrode–electrolyte interface, we divided the cross-section Raman map into seven parallel sectors and determined an average Raman spectrum for each region. Fig. 5B shows a series of average

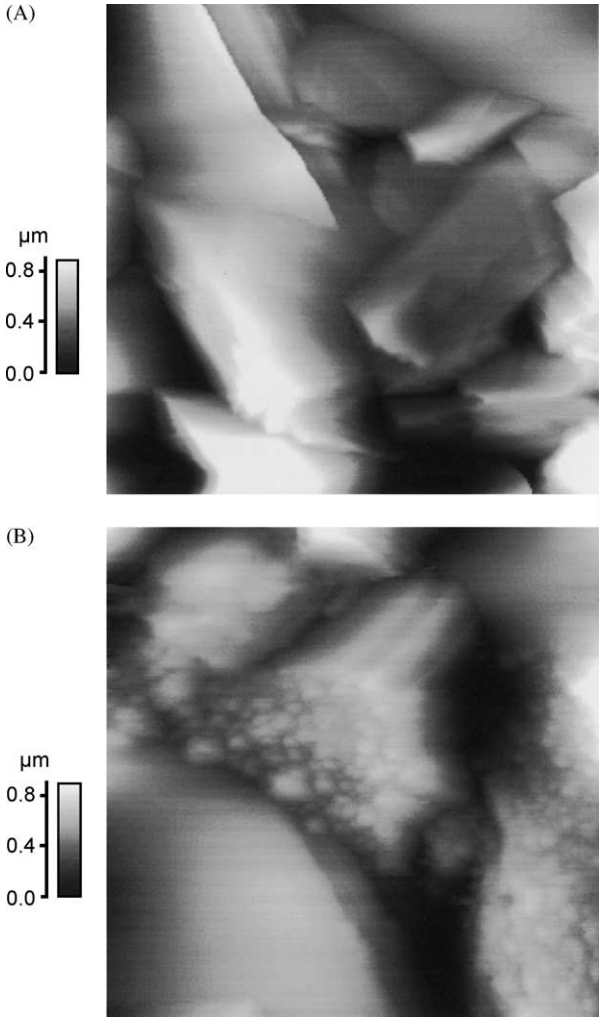

Fig. 4. AFM images (5 μm × 5 μm) of a fresh graphite anode (A) and the anode from the cell which was cycled at 60 °C (B).

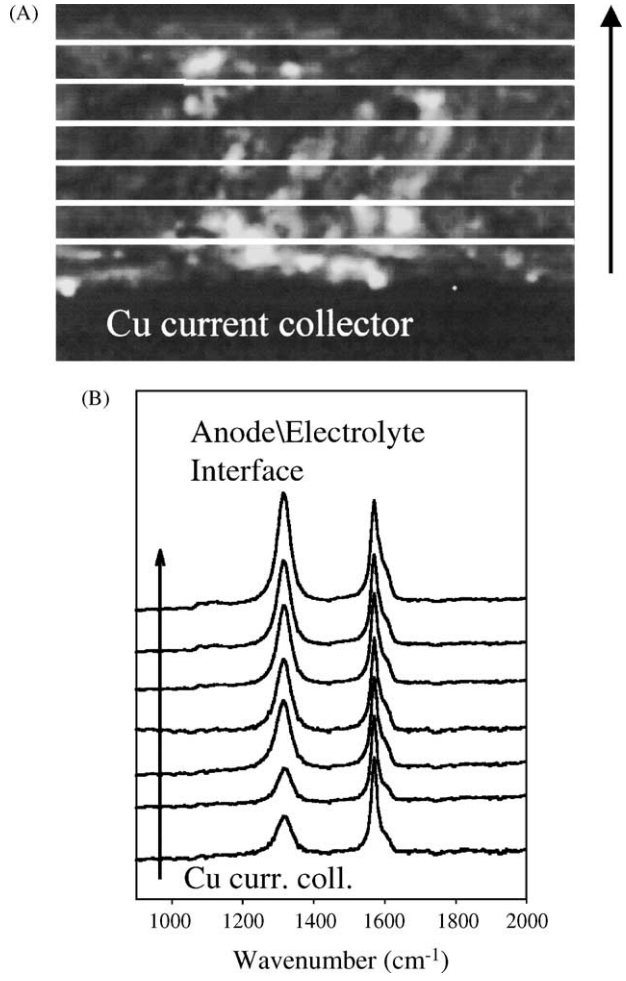

Fig. 5. (A) 50 μm × 75 μm cross-section Raman image portraying the graphite D/G band ratio of the anode which was cycled ∼140 times at 60 °C. White areas represent pure graphite and dark gray areas indicates structural disorder. (B) Average Raman spectra of the corresponding cross-section sub-layers.

Raman spectra from the corresponding anode sections. The Raman spectra display a very clear, monotonic trend. The graphite material close to the Cu current collector suffered much less damage than that near the anode/electrolyte interface. The transition from the fairly graphitic structure at the Cu/anode interface to severe disorder at the anode/electrolyte interface is gradual, as expressed by the steady increase of the D band intensity. Moreover, similar to what was observed at the anode surface, the more disordered is the local graphite material the stronger is the Raman signal at 1000–1200 cm^{-1}, which arises from inorganic electrolyte decomposition products. Thus, we present direct evidence that the presence of a SEI layer on graphite is not limited to the plane of the anode surface, but is rather associated with each individual graphite particle and is uniformly distributed across the anode bulk.

4. Discussion and conclusions

The lateral distribution of SEI compounds on the basal and cross-sectional planes of graphite particles after the cell formation process was determined by Peled et al. [20]. They found that the SEI on the graphitic plane cross-section is dominated by inorganic products whereas the basal planes are covered by a thin layer of organic polymers. Andresson and Edström [21] found that the SEI layer on graphite electrodes changes in both morphology and chemical composition during storage at elevated temperature mainly due to decomposition of the electrolyte salt. These observations are in concert with our Raman microscopy and AFM results. However, we found that the amount of inorganic decomposition products in the SEI layers of cycled anodes far exceeds that detected in the SEI of fresh anodes after the formation process. The increased thickness of the cross-section SEI is directly correlated in this case with the increasing graphite disorder, i.e. an increasing concentration of graphite edges, lattice defects etc., induced upon cycling at elevated temperature.

Local graphite degradation/exfoliation may be explained by the co-intercalation of ion aggregates and protons [20] or a localized high rate of lithium intercalation, both of which may arise from a non-uniform current distribution. This latter point is particularly noteworthy, because a non-uniform distribution of graphite structural disorder and/or inorganic decomposition products (both at the anode surface and in its bulk) suggests a corresponding non-uniform current density distribution across and within the anode. This correspondence implies that the graphite anode consists of sites that sustain current densities and reaction rates that are much higher than the average cell current would indicate. Either limited inter-granular electronic conductivity due to the presence of the SEI or limited Li-ion diffusion in partially blocked anode pores may be the root cause of such non-uniformities. Elevated temperature and cell cycling will eventually lead to graphite structure breakdown and the exposure of new graphitic edges and fragments of graphite planes. These freshly exposed active graphite sites are effective electrocatalysts and react readily with the electrolyte to form inorganic products such as phosphates, carbonates, and LiF. This process results the long-term accumulation of inorganic products at graphite particles, which form a barrier to Li-ion diffusion and thereby reduce cell power capabilities. Another detrimental aspect of this phenomenon is the gradual transfer of lithium from the cathode to the anode SEI, which eventually prevents full discharge of the cathode and thereby limits the Li-ion cell capacity.

Acknowledgements

This work was supported by the Assistant Secretary for Energy Efficiency and Renewable Energy, Office of FreedomCAR and Vehicle Technologies of the US Department of Energy under Contract No. DE-AC03-76SF00098.

References

[1] T. Zheng, J.R. Dahn, Applications of carbon in lithium-ion batteries, in: T.D. Burchell (Ed.), Carbon Material of Advanced Technology, Pergamon Press, Oxford, UK, 1999, p. 341.
[2] D. Aurbach, B. Markovsky, I. Weissman, E. Levi, Y. Ein-Eli, Electrochim. Acta 45 (1999) 67.
[3] A. Funabiki, M. Inaba, T. Abe, Z. Ogumi, Electrochim. Acta 45 (1999) 865.
[4] A.M. Andersson, K. Edström, J.O. Thomas, J. Power Sources 81/82 (1999) 8.
[5] I. Rey, J.-L. Bruneel, J. Grondin, L. Servant, J.-C. Lessegues, J. Electrochem. Soc. 145 (1998) 3034.
[6] Y. Luo, W.-B. Cai, D.A. Scherson, Electrochem. Solid State Lett. 4 (2001) A101.
[7] Y. Luo, W.-B. Cai, D.A. Scherson, J. Electrochem. Soc. 149 (2002) A1100.
[8] P. Novák, F. Joho, R. Imhof, J.-C. Panitz, O. Haas, J. Power Sources 81/82 (1999) 212.
[9] P. Novák, F. Joho, M. Lanz, B. Rykart, J.-C. Panitz, D. Alliata, R. Kötz, O. Haas, J. Power Sources 97/98 (2001) 39.
[10] J. Shim, R. Kostecki, T. Richardson, X. Song, K.A. Striebel, J. Power Sources 112 (2002) 222.
[11] Raymond A. Sutula et al., FY 2000 Progress Report for the Advanced Technology Development Program, US DOE, OAAT, December, 2000.
[12] R. Vidano, D.B. Fischbach, J. Am. Ceram. Soc. 61 (1978) 13.
[13] F. Tuinstra, J.L. Koenig, J. Chem. Phys. 53 (1976) 1126.
[14] M. Nakamizo, K. Tamai, Carbon 22 (1984) 197.
[15] F. Disma, L. Aymard, L. Dupont, J.-M. Tarascon, J. Electrochem. Soc. 143 (1996) 3959.
[16] T. Nakashima, M. Koh, M. Shimada, R. Shing, T. Shirasaki, A. Tressaud, in: International Symposium on Carbon Science and Technology for New Carbons, Japan, 1998, p. 396.
[17] Y. Ein-Eli, V.R. Koch, J. Electrochem. Soc. 144 (1997) 2968.
[18] P. Pasierb, S. Komornicki, M. Rokita, M. Rêkas, J. Mol. Struct. 596 (2001) 151.
[19] A.M. Efimov, J. Non-Cryst. Solids 253 (1999) 95, and references therein.
[20] E. Peled, D. Bar Tow, A. Merson, A. Gladkich, L. Burstein, D. Golodnitsky, J. Power Sources 97/98 (2001) 52.
[21] A.M. Andresson, K. Edström, J. Electrochem. Soc. 148 (2001) A1100.